RESEARCH ARTICLE

Check for updates

The potential of an MOF accelerator in an electrochemiluminescence system for sensitive detection of menthol enantiomers†

Xuan Kuang, [iD] *[a] Yeqian Ruan,[a] Jianping Xin[b] and Lin Lan*[a]

The critical element of an electrochemiluminescence (ECL) chiral sensor is the chiral electrode modifier. Its role is to selectively differentiate between enantiomers and convert this differentiation into an electrochemical signal. In this study, the researchers developed a chiral ECL recognition system for detecting menthol (Men). This system utilized a homochiral [(Zn(Hmim/L-His)$_2$)] (L-His-ZIF-8) as a coreactant accelerator and β-cyclodextrin (β-CD) as a chiral recognition inducer. By introducing coreactant promoters, the ECL efficiency was boosted to 34.7%, thereby improving the sensitivity of the chiral sensors. The researchers conducted a meticulous evaluation of β-CD's ability and mechanism for distinguishing chirality. The results demonstrated a significantly amplified ECL signal in the presence of L-Men, surpassing that of D-Men. This system exhibited exceptional selectivity, stability, and reproducibility in detecting the Men enantiomer and accurately identifying one Men enantiomer from a mixture. The research presents a reliable approach to achieve precise detection of chiral molecules, paving the way for advanced applications in chiral sensing and discrimination.

Introduction

Chirality is pivotal in diverse domains such as life sciences, food chemistry, and pharmaceutical production, as unique isomers can provoke a range of physiological responses, occasionally even diametrically opposed ones.[1,2] As such, chiral recognition is indeed regarded as one of the most intricate and avant-garde research topics within the realm of molecular recognition. Electrochemiluminescence (ECL) technology, with its high sensitivity, controllability, minimal background interference and cost-effectiveness, is extensively employed in clinical diagnosis and pharmaceutical analysis.[3–8] To address this challenge, researchers have been exploring the integration of chiral recognition elements with ECL systems. However, the creation of a chiral microenvironment for proficient enantioselective molecular recognition poses a formidable scientific challenge.[9,10] Adding to this complexity is the

endeavor of efficiently transposing this recognition to a discernible ECL signal response.

Cyclodextrins (CDs) are extensively utilized in biomedicine and pharmaceutical engineering for separation purposes, owing to their extraordinary ability to distinguish enantiomers and isomers.[11,12] β-Cyclodextrin (β-CD), a conformationally chiral macromolecule, is conferred its chirality by its constituent glucose units. The size and shape of the hydrophobic cavity endow it with the ability to form complexes with various chiral molecules through host–guest interactions.[13,14] However, the direct construction of ECL sensors using pure CDs is not ideal.[15] An effective ECL chiral sensor necessitates not only discrimination of each enantiomer but also a material that can distinguish and enhance the responsive signal.[16] The fusion of enantioselectivity and ECL properties endows the conjugated materials with a plethora of fascinating characteristics, rendering them ideal for utilization as sensing devices.

Typically, individual ECL luminophores struggle to produce a sufficiently robust signal due to self-annihilation. Enhancing the ECL signal is crucial for sensor sensitivity improvement, as it directly influences the output signal of the target.[17,18] Given that the generation of the ECL signal is contingent upon the interplay between the luminescent entity and the coreactant, which induces the emission of excited states, the amplification of the signal fundamentally hinges on the enhancement of this electrochemical reaction's efficiency.[19,20] A coreaction accelerator can be incorporated into the system to augment

[a] Key Laboratory of Interfacial Reaction & Sensing Analysis in Universities of Shandong, School of Chemistry and Chemical Engineering, University of Jinan, Jinan 250022, China. E-mail: chm_kuangx@ujn.edu.cn, Q1054248923@163.com
[b] Shandong Institute of Non-Metallic Materials, Jinan 250031, China

reaction efficiency.[21,22] This accelerator interacts with the co-reactant, generating more active intermediate states, thereby bolstering the ECL signal.[23,24] Recently, a number of coreaction accelerators have been put forward for different ECL coreaction systems, including nanomaterials,[25,26] single-atom materials,[27,28] organic small molecules,[29,30] and so on. However, the development of coreaction accelerators that are structurally simple, cost-effective, stable, and low in toxicity continues to pose a challenge.

Quantum dots (QDs), a type of luminescent nanomaterial, have gained significant attention in the realm of ECL biosensing due to their distinct emission spectra, high quantum yields, and affordability.[31,32] Nevertheless, their ECL efficiency remains inferior in comparison with those of traditional ECL reagents.[33,34] In this study, it was found that the addition of L-His-ZIF-8 to the L-CdS QDs/$S_2O_8^{2-}$ system significantly enhanced the ECL efficiency. The improvement observed can be ascribed to the combined effects of β-CD and L-His-ZIF-8. β-CD, as a substrate material, optimizes the loading of L-CdS QDs and prevents aggregation due to its inherent porosity and ultra-high surface area.[35,36] On the other hand, L-His-ZIF-8, as a core promoter, accelerates the reduction of co-reactant $S_2O_8^{2-}$, stimulating the production of more $SO_4^{\cdot-}$ species and thereby amplifying the luminescence intensity.

The study further elucidates that the enantiomers identified by β-CD can affect the loading of luminescent entities, enhancing the ECL signal and facilitating chiral differentiation. The integration of Men into the β-CD cavity impedes the dispersion of L-CdS QDs, resulting in a diminished ECL signal.[37–39] This research presents the potential of chiral recognition probes and coreaction promoters as sensing platforms for augmenting ECL signals and achieving selective and sensitive detection of chiral enantiomers. This strategy holds significant promise for the development of innovative chiral detection methods in various applications.

Experimental section

Preparation of L-CdS QDs

The synthesis of L-Cys capped CdS QDs (L-CdS QDs) was carried out following a previously established method.[40] Briefly, $CdCl_2·2.5H_2O$ (0.183 g, 0.4 mmol), L-Cys (0.242 g, 2.0 mmol) and $Na_2S·9H_2O$ (0.508 g, 3.0 mmol) were added to ultrapure H_2O (70 mL) at ambient temperature. This mixture was then heated at 70 °C for 8 h under reflux and stirring conditions. After cooling, the resulting L-CdS QDs underwent purification through centrifugation and washed three times with EtOH and ultrapure H_2O. These purified L-CdS QDs were then dispersed in 80 mL of ultrapure H_2O using ultrasound and placed at 4 °C for future applications.

Preparation of L-His-ZIF-8

The synthesis of L-His-ZIF-8 was carried out using a classical method reported originally.[41] L-His (0.145 g, 1.2 mmol) and Hmim (0.673 g, 8.2 mmol) were dissolved in 25 mL of ultra-pure water, supplemented with 100 μL of triethylamine (TEA), and stirred for 10 minutes. Separately, $Zn(NO_3)_2·6H_2O$ (0.714 g, 2.4 mmol) was added to 30 mL of ultrapure H_2O and stirred for 5 min. The two solutions were combined and stirred at ambient temperature for 24 h. The resulting product was collected by centrifugation at 7000 rpm for 5 minutes, subjected to three washes with methanol, and dried overnight at 60 °C.

Fabrication process of the ECL sensor

Prior to modification, a glassy carbon electrode (GCE) with a diameter of 4 mm was polished and cleaned with ethanol and ultrapure water. A homogeneous film was formed on the electrode surface by adding 10 μL of 0.3 wt% Nafion solution containing β-CD dispersion (0.1 mmol mL^{-1}). Subsequently, a specific volume of the isomer was adsorbed onto the modified electrode, designed to interact with the chiral sites within the β-CD matrix. The modified GCE was immersed in ultrapure H_2O to remove any non-specifically adsorbed species after each step of the modification procedure. Following this, 10 μL of L-CdS QDs was further added onto the GCE surface. Finally, the aforementioned electrode underwent incubation with a 0.3 wt% Nafion solution, which consisted of L-His-ZIF-8 at a concentration of 1.5 mg mL^{-1}. Subsequently, it was left to dry at room temperature.

Results and discussion

Structure and characterization

The transmission electron microscopy (TEM) technique was employed to characterize the micromorphologies of L-CdS quantum dots (QDs). The obtained results, illustrated in Fig. 1A and B, show well-defined globular structures of L-CdS QDs, with clearly visible crystal stripes. The fringe spacing measurement in Fig. 1B corresponds to a value of 2.4 Å, which
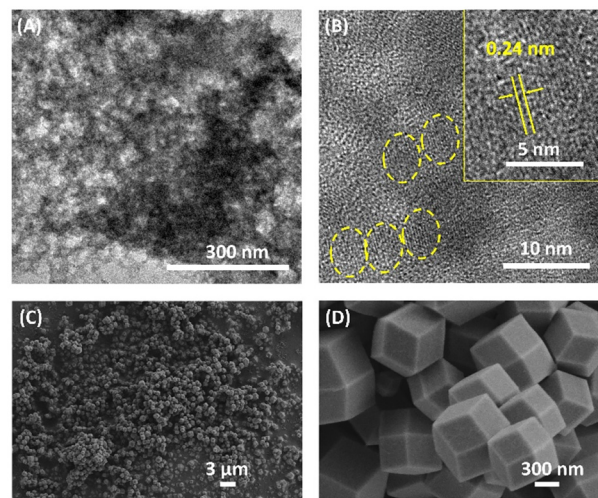

Fig. 1 (A) and (B) TEM images of L-CdS QDs. (C) and (D) SEM images of L-His-ZIF-8 at different magnifications.

4242 | *Inorg. Chem. Front.*, 2024, **11**, 4241–4248

This journal is © the Partner Organisations 2024

is consistent with that of the (102) crystal plane of a hexagonal CdS crystal (d = 2.45 Å). Moreover, the UV-vis absorption spectrum illustrated in Fig. S1† displays a broad absorption band ranging from 400 to 500 nm for L-CdS QDs. Additionally, the fluorescence emission spectrum of L-CdS QDs exhibits a central peak at 503 nm, indicating a highly uniform particle size. These pieces of evidence show the successful synthesis of L-CdS QD nanoparticles. Further characterization using scanning electron microscopy (SEM) reveals that the L-His-ZIF-8 particles are nanocrystals with hexagonal facets, demonstrating a relatively uniform size distribution of approximately 700 nm (Fig. 1C and D).

Fig. 2A presents the powder X-ray diffractometry (PXRD) pattern of the synthesized L-His-ZIF-8, aligning with the simulated pure-phase L-His-ZIF-8. The FT-IR spectrum in Fig. 2B reveals a sharp peak at approximately 1627 cm^{-1} in the L-His-ZIF-8 spectrum, attributable to the stretching vibrations of the C=O bond in the carboxy group of L-His. Another absorption peak at 1057 cm^{-1} associated with the amine group on the side chain of L-His further validates the effective integration of L-His and ZIF-8.

ECL behaviors of the GCE modified with different samples

Cyclic voltammetry (CV) and electrochemical impedance spectroscopy (EIS) were adopted to illustrate the stepwise fabrication process of the sensor. As seen in Fig. S2A,† a distinct reversible redox pair appears at the bare GCE. This redox pair is associated with the electrochemical interconversion between $[Fe(CN)_6]^{3-}$ and $[Fe(CN)_6]^{4-}$, which aligns with the initial scan. Following β-CD modification of the electrode, the redox peak current is noticeably reduced owing to the limited electrochemical activity of β-CD, and the electron transfer of quantum dots is limited. The increase in the redox peaks of the β-CD/L-CdS QDs/GCE is not significant, and the current signal of the β-CD/L-CdS QDs/L-His-ZIF-8/GCE continues to diminish, likely due to the low conductivity of L-His ZIF-8. The corresponding EIS analysis is presented in Fig. S2B.† The Nyquist plot clearly shows a marked decrease in the resistance of the β-CD/L-CdS QDs/L-His-ZIF-8/GCE when compared to those of the bare GCE, β-CD/GCE, and β-CD/L-CdS QDs/GCE, which is in agreement with the CV results.
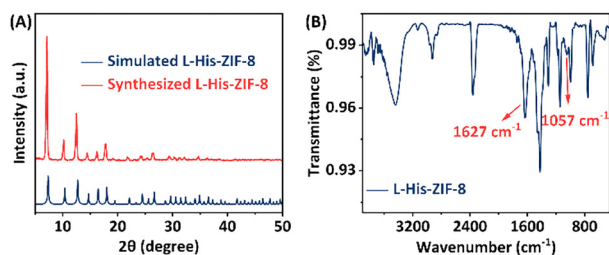
Fig. 2 (A) XRD patterns of simulated L-His-ZIF-8 (blue) and synthesized L-His-ZIF-8 (orange). (B) FT-IR spectrum of L-His-ZIF-8.
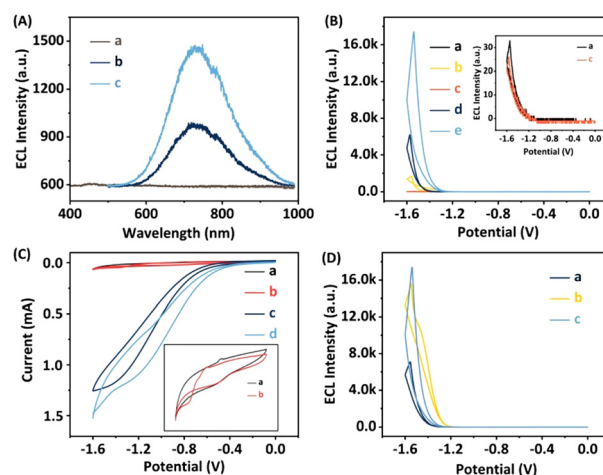
Fig. 3 (A) ECL spectra of various modified GCEs in 0.1 M PBS (pH 7.4): (curve a) L-His-ZIF-8 + $S_2O_8^{2-}$, (curve b) L-CdS QDs + $S_2O_8^{2-}$ and (curve c) L-CdS QDs + L-His-ZIF-8 + $S_2O_8^{2-}$. (B) ECL intensity−potential curves of (curve a) the bare GCE, (curve b) L-CdS QDs/GCE, (curve c) β-CD/GCE, (curve d) β-CD/L-CdS QDs/GCE and (curve e) β-CD/L-CdS QDs/L-His-ZIF-8/GCE in 0.1 M PBS of pH 7.4 containing 0.1 M $K_2S_2O_8$. (C) CV responses of various modified electrodes in 0.1 M PBS (pH 7.4): (curve a) β-CD + L-CdS QDs, (curve b) β-CD + L-CdS QDs + L-His-ZIF-8, (curve c) β-CD + L-CdS QDs + $S_2O_8^{2-}$ and (curve d) β-CD + L-CdS QDs + L-His-ZIF-8 + $S_2O_8^{2-}$. (D) ECL intensity−potential curves of the β-CD/L-CdS QDs/L-His-ZIF-8/GCE in 0.1 M PBS (pH 7.4) containing 0.1 M $K_2S_2O_8$ (curve c) with and without 0.1 mM (curve a) D-Men or (curve b) L-Men.
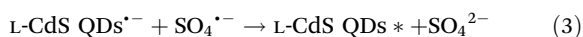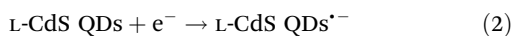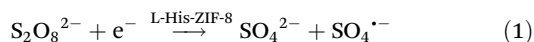
Possible ECL mechanism

To identify the luminescent agent and further elucidate the ECL reaction mechanism of the proposed system, both ECL and CV measurements were conducted, as depicted in Fig. 3. The results reveal minimal spectral fluctuations in the ECL emission spectrum of L-His-ZIF-8 + $S_2O_8^{2-}$, implying the absence of luminescent groups within L-His-ZIF-8. Meanwhile, the ECL emission spectrum of the L-CdS QDs + $S_2O_8^{2-}$ solution exhibits a peak emission wavelength at 700 nm (Fig. 3A, curve b), consistent with the hypothesis that the emitted light originates from the excited state of L-CdS QDs (L-CdS QDs*) with $S_2O_8^{2-}$ as the coreactant in the L-CdS QDs/$S_2O_8^{2-}$ system.[42,43] Intriguingly, the peak emission wavelength of the L-CdS QDs + $S_2O_8^{2-}$ + L-His-ZIF-8 solution remains at 700 nm (Fig. 3A, curve c), indicating that the luminescent agent in the L-CdS QDs/L-His-ZIF-8 ECL system is L-CdS QDs, rather than the singlet state oxygen ($^1(O_2)_2$*) in the $S_2O_8^{2-}$ solution.[44,45] Moreover, the ECL intensity experiences a significant amplification in the L-CdS QDs + $S_2O_8^{2-}$ + L-His-ZIF-8 solution, indicating that L-His-ZIF-8 has the potential to enhance the intensity of the L-CdS QDs/$S_2O_8^{2-}$ ECL system. This implies that L-His-ZIF-8 acts as a coreaction accelerator for L-CdS QDs/$S_2O_8^{2-}$ in this ternary system.

To assess the effectiveness of the suggested approach, the ECL responses of different electrodes were compared under the same experimental conditions. The evaluations were conducted in 0.1 M phosphate-buffered saline (PBS) at pH 7.4, with 0.1 M $K_2S_2O_8$ serving as the coreaction reagent. From

This journal is © the Partner Organisations 2024

Inorg. Chem. Front., 2024, **11**, 4241–4248 | **4243**

Fig. 3B, it can be observed that both the bare GCE and L-His-ZIF-8/GCE did not exhibit any significant ECL signal. In contrast, the ECL signal of the β-CD/L-CdS QDs/L-His-ZIF-8/GCE was approximately 17416 arbitrary units (a.u.), which is 2.8-fold greater than that of the β-CD/L-CdS QDs/GCE (~6186 a.u.) and 10.4-fold higher than that of the L-CdS QDs/GCE (~1676 a. u.). This further suggests that L-His-ZIF-8 serves as a co-reaction accelerator for the L-CdS QDs/$S_2O_8^{2-}$ ECL system, and the inclusion of β-CD does not impact the ECL signal.

As illustrated in Fig. 3C, a quartet of distinct CV responses were meticulously documented. The CV curve of the β-CD + L-CdS QD solution (curve a) manifests a pair of redox peaks. The infusion of L-His-ZIF-8 into this concoction leaves the redox peak unaltered (curve b), suggesting a lack of reaction between L-His-ZIF-8 and the luminescent entity. A redox peak emerges in the β-CD + L-CdS QDs + $S_2O_8^{2-}$ solution (curve c) due to the interaction between $S_2O_8^{2-}$ and L-CdS QDs, giving rise to an overpotential increase. By the incorporation of L-His-ZIF-8 into this system, the redox peak current (curve d) markedly amplifies, indicating that L-His-ZIF-8 can facilitate the oxidation reaction between L-CdS QDs and $S_2O_8^{2-}$. Subsequently, the ECL efficiency of the β-CD/L-CdS QDs/L-His-ZIF-8 system was calculated. The results showed that the ECL efficiency of the system was 34.7%, compared to that of standard Ru (bpy)$_3$Cl$_2$/K$_2$S$_2$O$_8$ (the calculation procedure is shown in the ESI†).

The reaction mechanism can be summarized according to the previously established luminescence pathway as follows:

$$S_2O_8^{2-} + e^- \xrightarrow{\text{L-His-ZIF-8}} SO_4^{2-} + SO_4^{\bullet-} \tag{1}$$

$$\text{L-CdS QDs} + e^- \rightarrow \text{L-CdS QDs}^{\bullet-} \tag{2}$$

$$\text{L-CdS QDs}^{\bullet-} + SO_4^{\bullet-} \rightarrow \text{L-CdS QDs} * + SO_4^{2-} \tag{3}$$

$$\text{L-CdS QDs*} \rightarrow \text{L-CdS QDs} + h\nu \tag{4}$$

The presence of L-His-ZIF-8 is essential in facilitating the electroreduction process of $S_2O_8^{2-}$ to $SO_4^{\bullet-}$ and SO_4^{2-} (eqn (1)),[30] while facilitating the transfer of electrons from the GCE to L-CdS QDs. This electron transfer results in the formation of the excited state L-CdS QDs$^{\bullet-}$ (eqn (2)). Further interaction between the potent oxidant species ($SO_4^{\bullet-}$) and L-CdS QDs$^{\bullet-}$ leads to the creation of L-CdS QDs* (eqn (3)). The relaxation of the excited state L-CdS QDs* back to the ground state L-CdS QDs gives rise to the detection of ECL intensity (eqn (4)).

Chiral discrimination of Men utilizing the developed ECL system

By examining the ECL intensity–potential curves of the β-CD/L-CdS QDs/L-His-ZIF-8/GCE in a 0.1 M PBS solution with pH 7.4, containing either 0.1 mM D-Men or L-Men for a duration of 5 minutes (Fig. 3D), it was observed that the β-CD/L-CdS QDs/L-His-ZIF-8/GCE exhibited significantly higher ECL signals with L-Men compared to those obtained with D-Men.

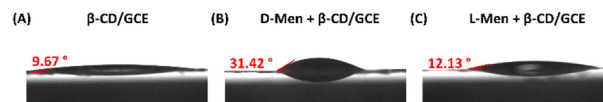The affinity of β-CD for Men enantiomers was validated through the evaluation of the wettability of disparate samples,

Fig. 4 Photographic comparison of water contact angles on sheets of (A) pure β-CD and β-CD after being immersed in either (B) D-Men or (C) L-Men solutions.

as shown in Fig. 4. It suggests that the β-CD refrains from adsorbing excessive quantities of L-Men, thereby maintaining its inherent hydrophilicity and presenting a contact angle similar to that of pure β-CD. Conversely, the interaction between D-Men and β-CD has a profound effect on the surface hydrophilicity of β-CD, causing its decrease significantly.

Circular Dichroism (CD) was employed to further investigate the adsorption behavior of β-CD on Men isomers. The CD spectra depicted in Fig. S3† shed light on β-CD's interactions with L- or D-Men. After adsorbing equal amounts of L-/D-Men, the residual traces were removed from β-CD by treating it with EtOH. Notably, as β-CD lacks a CD signal, only the distinctive CD signal of Men was discernible in the experimental results.[46] The absence of CD signals in both β-CD and β-CD + L-Men spectra, contrasted with the presence of a CD signal in β-CD + D-Men, indicates the preferential interaction and binding of D-Men over L-Men by the β-CD molecules.

The molecular behavior of L-/D-Men in the presence of β-CD was investigated using Density Functional Theory (DFT). The adsorption of both L-/D-Men onto β-CD primarily occurs through hydrogen bonding, while van der Waals forces also contribute to a lesser extent. The distances between the hydroxyl group of Men and β-CD, measured as O–H···O, were found to be 1.82 Å for L-Men and 1.91 Å for D-Men (Fig. 5). However, the formation of these hydrogen bonds leads to increased steric hindrance between the remaining group of L-Men and β-CD, resulting in a less stable adsorption energy compared to that of D-Men. The calculation reveals that L-Men has a binding energy of −19.97 kcal mol^{-1}, while D-Men has a binding energy of −22.35 kcal mol^{-1}. This indicates that D-Men exhibits a more favorable adsorption to β-CD due to its more negative binding energy.
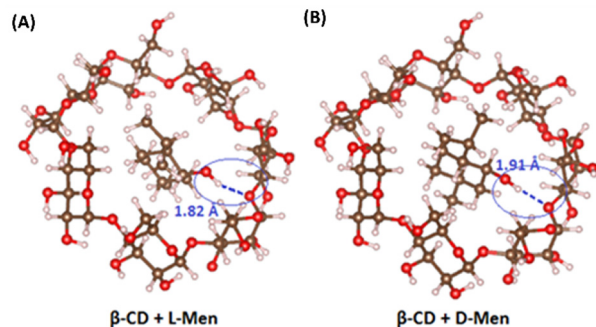

Fig. 5 Characterization of the adsorption behavior and binding energy between β-CD and (A) L-Men and (B) D-Men.

4244 | *Inorg. Chem. Front.,* 2024, **11**, 4241–4248

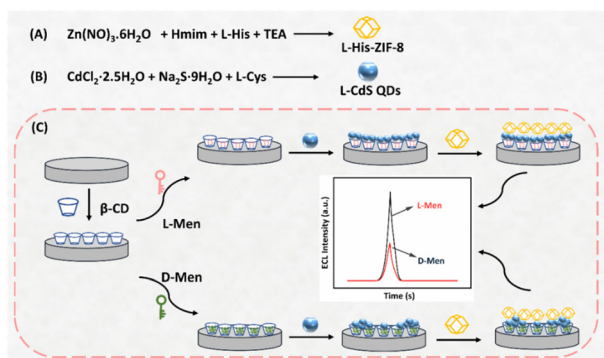This journal is © the Partner Organisations 2024

Fig. 6 Visual representation demonstrating the mechanisms responsible for chiral discrimination in ECL.

Fig. 6 depicts the chiral discrimination mechanism in ECL, based on the experimental findings discussed earlier. We noted a weaker interaction between L-Men and the β-CD/L-CdS QDs/L-His-ZIF-8/GCE, resulting in a higher ECL intensity value for β-CD + L-CdS QDs + L-His-ZIF-8 compared to that of its D-Men counterpart. This phenomenon could be explained by the existence of distinct binding sites within β-CD, which potentially foster a higher affinity of D-Men towards β-CD compared to that of L-Men. When Men is incorporated into the cavity of β-CD, it obstructs the entry of L-CdS QDs, leading to their aggregation, which ultimately diminishes ECL efficiency. Meanwhile, L-His-ZIF-8 facilitates the redox reaction between the L-CdS QDs and the co-reagent, thereby enhancing the ECL signal and amplifying the signal difference.

The optimization of experimental conditions

An optimization experiment was conducted to determine the optimal concentration of β-CD, considering its potential influence on the conductivity of the electrode and subsequent impact on the ECL signal (Fig. S4A†). It was found that excessively high concentrations of β-CD led to a decline in the conductivity of the electrode, which in turn reduced the ECL signal. Conversely, inadequate concentrations of β-CD resulted in a diminished ability to adsorb Men enantiomers. The ECL signal obtained indicated that the optimal performance was achieved with a β-CD concentration of 0.1 mmol mL^{-1}. Moreover, meticulous calibration of the L-His-ZIF-8 concentration was conducted to amplify the recognition efficiency of the β-CD/L-CdS QDs/L-His-ZIF-8/GCE system towards Men (Fig. S4B†). It was determined that an L-His-ZIF-8 concentration of 1.5 mg mL^{-1} led to a high recognition efficiency for Men. To attain an adequate ECL intensity, the pH value of 0.1 M K$_2$S$_2$O$_8$–0.1 M PBS solutions was optimized using β-CD incubated with 0.1 mM Men isomers. The ECL intensity variations, depicted in Fig. S4C,† across pH values ranging from 5.6 to 8.04 suggest that the highest intensity is observed in alkaline solutions. The elevated pH levels promote the formation of stronger hydrogen bonds between Men and β-CD, thereby reducing interactions with both L-Men and D-Men. Moreover, the difference in ECL intensity ($Δ_{EI}$) was found to be most pro-

nounced at pH 7.4 compared to other pH values. As a result, pH 7.4 was selected as the optimal buffer solution for subsequent experiments, based on its ability to maximize the distinction in ECL signals.

The system's ability to accurately measure L-Men and D-Men concentrations was evaluated using optimized conditions. Within the concentration range of 50 nM to 0.1 mM, a clear and linear correlation between the ECL signal and the L/D-Men concentration was observed, with the ECL signal decreasing as the concentrations of L/D-Men increased (Fig. 7A and B). The linear regression equations were derived as I_{L-Men} = −1729.88 lg C (μM) + 13296.93 (R^2 = 0.9982) and I_{D-Men} = −904.98 lg C (μM) + 5865.58 (R^2 = 0.9961). On the basis of a signal-to-noise ratio of 3 (S/N = 3), the limit of detection (LOD) for both L-Men and D-Men was calculated to be 0.046 μM. These results emphasise the considerable potential of the envisaged approach to achieve a highly sensitive and stereoselective detection of Men isomers. In addition, this system exhibits a stronger ECL signal difference for the same concentration of isomers, and the LOD is significantly lower than those of some ECL chiral sensors (Table S1, ESI†), indicating that its recognition ability for chiral enantiomers is more efficient and sensitive.

Selectivity, stability, and reproducibility of the ECL system

The reproducibility and stability of the proposed ECL platform for distinguishing between Men isomers were thoroughly examined. The analysis of Fig. 7C and D revealed that both L-Men and D-Men demonstrated minimal fluctuations in the ECL signals during successive cyclic potential scans (n = 10), with RSDs of 0.32% and 1.37%, respectively. These results emphasize the exceptional stability of the ECL platform. Additionally, when three separate β-CD/L-CdS QDs/L-His-ZIF-8/
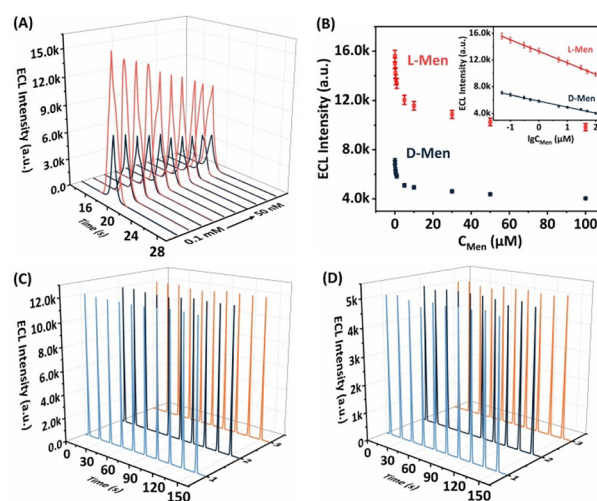

Fig. 7 (A) ECL curves of the constructed sensor toward the detection of L-Men and D-Men with various concentrations from 50 nM to 0.1 mM. (B) Calibration plot for the ECL intensity *versus* the logarithm of target concentrations. Stability and reproducibility evaluation of the β-CD/L-CdS QDs/L-His-ZIF-8/GCE with (C) L-Men and (D) D-Men.

GCE preparations were tested under identical conditions, the ECL signals remained virtually unchanged during the 10th measurement. The RSD values for ʟ-Men and ᴅ-Men were 0.20% and 1.04%, respectively, confirming the impressive reproducibility of the system. Consequently, the developed ECL platform can be deemed a dependable tool for detecting Men enantiomers.

To assess the specificity of the proposed approach, a range of sixteen enantiomers were chosen for comparison at a concentration of 0.1 mM. These enantiomers encompassed phenylalanine (Phe), threonine (Thr), tyrosine (Tyr), serine (Ser), glutamic acid (Glu), alanine (Ala), arginine (Arg), proline (Pro), tryptophan (Trp), methionine (Met), mandelic acid (Man), valine (Val), penicillamine (PA), carnitine (Car), naproxen (Nap), and aspartic acid (Asp). As depicted in Fig. S5,† the Δ_{EI} values exhibited marginal disparaties between these enantiomers, and the ECL signals remained practically unaltered in comparison with those of the baseline sample. This compelling proof corroborates the selective recognition capability of the proposed method towards Men enantiomers.

Application of the enantioselective electrode

To evaluate the practical performance of the established chiral recognition system, the β-CD/ʟ-CdS QDs/ʟ-His-ZIF-8/GCE was applied to resolve a racemic mixture of Men isomers with a total concentration of 0.1 mM *via* ECL. Interestingly, the two ECL signals of ᴅ- and ʟ-Men converged into a single signal. However, a clear correlation was observed between the ECL signals and the percentage of ʟ-Men in the racemic mixture. This demonstrates the system's ability to accurately recognize one enantiomer of Men in the mixture (Fig. S6†), further highlighting the practical applicability of the developed chiral recognition system.

Conclusions

In conclusion, a novel chiral ECL recognition strategy was developed based on a multifunctional β-CD/ʟ-CdS QDs/ʟ-His-ZIF-8/GCE. Besides functioning as a chiral recognition sensor, this system also serves as a co-acting accelerator, enhancing the ECL signal of the luminescent materials. This dual functionality meets the requirements for high sensitivity and convenient labeling of ECL signals. The constructed ECL system demonstrated a low detection limit, exceptional sensitivity, a wide linear range, and acceptable stability in Men analysis. Given these advantages, this co-reaction accelerator amplification approach holds great potential for the development of highly sensitive sensing platforms based on low-intensity luminescent materials.

Author contributions

X. Kuang conceptualized and designed the study, and reviewed and edited the manuscript. L. Lan conducted the experiments, collected the data, and wrote the original draft of the manuscript. Y. Q. Ruan performed the data analysis and interpretation. J. P. Xin contributed to the development of the methodology. All authors have given approval to the final version of the manuscript.

Conflicts of interest

The authors declare that they have no known competing financial interests or personal relationships that could have appeared to influence the work reported in this paper.

Acknowledgements

References

1 X.-L. Yang, Z.-Y. Yang, R. Shao, R.-F. Guan, S.-L. Dong and M.-H. Xie, Chiral MOF Derived Wearable Logic Sensor for Intuitive Discrimination of Physiologically Active Enantiomer, *Adv. Mater.*, 2023, 2304046.

2 Y. Liu, Z. Wu, D. W. Armstrong, H. Wolosker and Y. Zheng, Detection and analysis of chiral molecules as disease biomarkers, *Nat. Rev. Chem.*, 2023, **7**, 355–373.

3 A. Barhoum, Z. Altintas, K. S. S. Devi and R. J. Forster, Electrochemiluminescence biosensors for detection of cancer biomarkers in biofluids: Principles, opportunities, and challenges, *Nano Today*, 2023, **50**, 101874.

4 Y. Cao, J.-X. Wang, C. Lin, Y.-Q. Geng, C. Ma, J.-J. Zhu, L. Wang and W. Zhu, Zwitterionic Electrochemiluminescence Biointerface Contributes to Label-Free Monitoring of Exosomes Dynamics in a Fluidic Microreaction Device, *Adv. Funct. Mater.*, 2023, **33**, 2214294.

5 K. Wu, R. Chen, Z. Zhou, X. Chen, Y. Lv, J. Ma, Y. Shen, S. Liu and Y. Zhang, Elucidating Electrocatalytic Oxygen Reduction Kinetics via Intermediates by Time-Dependent Electrochemiluminescence, *Angew. Chem., Int. Ed.*, 2023, **62**, e202217078.

6 Y. Hou, Y. Fang, Z. Zhou, Q. Hong, W. Li, H. Yang, K. Wu, Y. Xu, X. Cao, D. Han, S. Liu, Y. Shen and Y. Zhang, Growth of Robust Carbon Nitride Films by Double Crystallization with Exceptionally Boosted Electrochemiluminescence for Visual DNA Detection, *Adv. Opt. Mater.*, 2023, **11**, 2202737.

7 Q. Sun, Z. Ning, E. Yang, F. Yin, G. Wu, Y. Zhang and Y. Shen, Ligand-induced Assembly of Copper Nanoclusters with Enhanced Electrochemical Excitation and Radiative Transition for Electrochemiluminescence, *Angew. Chem., Int. Ed.*, 2023, **62**, e202312053.

8 T. Zhao, Q. Zhou, Y. Lv, D. Han, K. Wu, L. Zhao, Y. Shen, S. Liu and Y. Zhang, Ultrafast Condensation of Carbon Nitride on Electrodes with Exceptional Boosted

4246 | *Inorg. Chem. Front.*, 2024, **11**, 4241–4248

This journal is © the Partner Organisations 2024

Photocurrent and Electrochemiluminescence, *Angew. Chem., Int. Ed.*, 2020, **59**, 1139–1143.

9 M.-Y. Wu, R.-J. Mo, X.-L. Ding, L.-Q. Huang, Z.-Q. Li and X.-H. Xia, Homochiral Zeolitic Imidazolate Framework with Defined Chiral Microenvironment for Electrochemical Enantioselective Recognition, *Small*, 2023, **19**, 2301460.

10 G. Yang, W. Shi, Y. Qian, X. Zheng, Z. Meng and H.-L. Jiang, Turning on Asymmetric Catalysis of Achiral Metal-Organic Frameworks by Imparting Chiral Microenvironment, *Angew. Chem., Int. Ed.*, 2023, **62**, e202308089.

11 M. Singh, R. Sharma and U. C. Banerjee, Biotechnological applications of cyclodextrins, *Biotechnol. Adv.*, 2002, **20**, 341–359.

12 C. Guo and Y. Xiao, Negatively charged cyclodextrins: Synthesis and applications in chiral analysis-A review, *Carbohydr. Polym.*, 2021, **256**, 117517.

13 L. Chen, Y. Chen, Y. Zhang and Y. Liu, Photo-Controllable Catalysis and Chiral Monosaccharide Recognition Induced by Cyclodextrin Derivatives, *Angew. Chem., Int. Ed.*, 2021, **60**, 7654–7658.

14 H. Hanayama, J. Yamada, I. Tomotsuka, K. Harano and E. Nakamura, Rim Binding of Cyclodextrins in Size-Sensitive Guest Recognition, *J. Am. Chem. Soc.*, 2021, **143**, 5786–5792.

15 Y. Wang, Y. Li, X. Zhuang, C. Tian, X. Fu and F. Luan, Ru (bpy)32+ encapsulated cyclodextrin based metal organic framework with improved biocompatibility for sensitive electrochemiluminescence detection of CYFRA21–1 in cell, *Biosens. Bioelectron.*, 2021, **190**, 113371.

16 Q. Zhao, W. Zhu, W. Cai, J. Li, D. Wu and Y. Kong, TiO2 Nanotubes Decorated with CdSe Quantum Dots: A Bifunctional Electrochemiluminescent Platform for Chiral Discrimination and Chiral Sensing, *Anal. Chem.*, 2022, **94**, 9399–9406.

17 X. Gao, G. Jiang, C. Gao, A. Prudnikau, R. Hübner, J. Zhan, G. Zou, A. Eychmüller and B. Cai, Interparticle Charge-Transport-Enhanced Electrochemiluminescence of Quantum-Dot Aerogels, *Angew. Chem., Int. Ed.*, 2023, **62**, e202214487.

18 X. Ouyang, Y. Wu, L. Guo, L. Li, M. Zhou, X. Li, T. Liu, Y. Ding, H. Bu, G. Xie, J. Shen, C. Fan and L. Wang, Self-assembly Induced Enhanced Electrochemiluminescence of Copper Nanoclusters Using DNA Nanoribbon Templates, *Angew. Chem., Int. Ed.*, 2023, **62**, e202300893.

19 N. Wang, H. Gao, Y. Li, G. Li, W. Chen, Z. Jin, J. Lei, Q. Wei and H. Ju, Dual Intramolecular Electron Transfer for In Situ Coreactant-Embedded Electrochemiluminescence Microimaging of Membrane Protein, *Angew. Chem., Int. Ed.*, 2021, **60**, 197–201.

20 D. Zhu, Y. Zhang, S. Bao, N. Wang, S. Yu, R. Luo, J. Ma, H. Ju and J. Lei, Dual Intrareticular Oxidation of Mixed-Ligand Metal–Organic Frameworks for Stepwise Electrochemiluminescence, *J. Am. Chem. Soc.*, 2021, **143**, 3049–3053.

21 Y. Nie, Y. Liu, Q. Zhang, X. Su and Q. Ma, Novel coreactant modifier-based amplified electrochemiluminescence sensing method for point-of-care diagnostics of galactose, *Biosens. Bioelectron.*, 2019, **138**, 111318.

22 Y.-Q. Xue, N. Liao, Y. Li, W.-B. Liang, X. Yang, X. Zhong and Y. Zhuo, Ordered heterogeneity in dual-ligand MOF to enable high electrochemiluminescence efficiency for bioassay with DNA triangular prism as signal switch, *Biosens. Bioelectron.*, 2022, **217**, 114713.

23 N. Liao, M.-C. Pan, J.-F. Chen, X. Zhong, R. Yuan and Y. Zhuo, A dual engine-triggered DNA walker based on luminous perylene-TiO2 nanospheres for efficient electrochemiluminescence bioassay, *Chem. Eng. J.*, 2022, **450**, 138284.

24 H. Wang, Y. Wang, L. Cai, C. Liu, B. Zhang, G. Fang and S. Wang, Polythionine-mediated AgNWs-AuNPs aggregation conductive network: Fabrication of molecularly imprinted electrochemiluminescence sensors for selective capture of kanamycin, *J. Hazard. Mater.*, 2022, **434**, 128882.

25 J. Li, M. Luo, H. Yang, R. Cai and W. Tan, AuPt Nanodonuts as a Novel Coreaction Accelerator and Luminophore for a Label-free Electrochemiluminescence Aptasensor, *Anal. Chem.*, 2023, **95**, 13838–13843.

26 J.-L. Liu, Z.-L. Tang, Y. Zhuo, Y.-Q. Chai and R. Yuan, Ternary Electrochemiluminescence System Based on Rubrene Microrods as Luminophore and Pt Nanomaterials as Coreaction Accelerator for Ultrasensitive Detection of MicroRNA from Cancer Cells, *Anal. Chem.*, 2017, **89**, 9108–9115.

27 Z. Luo, W. Xu, Z. Wu, L. Jiao, X. Luo, M. Xi, R. Su, L. Hu, W. Gu and C. Zhu, Iron Single-Atom Catalyst-Enabled Peroxydisulfate Activation Enhances Cathodic Electrochemiluminescence of Tris(bipyridine)ruthenium (II), *Anal. Chem.*, 2023, **95**, 10762–10768.

28 W. Gu, X. Wang, M. Xi, X. Wei, L. Jiao, Y. Qin, J. Huang, X. Cui, L. Zheng, L. Hu and C. Zhu, Single-Atom Iron Enables Strong Low-Triggering-Potential Luminol Cathodic Electrochemiluminescence, *Anal. Chem.*, 2022, **94**, 9459–9465.

29 X. Jiang, H. Wang, Y. Chai, W. Shi and R. Yuan, High-Efficiency CNNS@NH2-MIL(Fe) Electrochemiluminescence Emitters Coupled with Ti3C2 Nanosheets as a Matrix for a Highly Sensitive Cardiac Troponin I Assay, *Anal. Chem.*, 2020, **92**, 8992–9000.

30 Q. Han, C. Wang, Z. Li, J. Wu, P. k. Liu, F. Mo and Y. Fu, Multifunctional Zinc Oxide Promotes Electrochemiluminescence of Porphyrin Aggregates for Ultrasensitive Detection of Copper Ion, *Anal. Chem.*, 2020, **92**, 3324–3331.

31 S. Yu, Y. Du, X. Niu, G. Li, D. Zhu, Q. Yu, G. Zou and H. Ju, Arginine-modified black phosphorus quantum dots with dual excited states for enhanced electrochemiluminescence in bioanalysis, *Nat. Commun.*, 2022, **13**, 7302.

32 L. Liu, Y. Xu, Y. Zhu, H. Wang, Y. Chai and R. Yuan, Near-infrared electrochemiluminescence of carbon nitride

This journal is © the Partner Organisations 2024

Inorg. Chem. Front., 2024, **11**, 4241–4248 | **4247**

quantum dots for ultrasensitive microRNA assay, *Chem. Eng. J.*, 2023, **472**, 145107.

33 L. Li, W. Zhao, J. Zhang, L. Luo, X. Liu, X. Li, T. You and C. Zhao, Label-free Hg(II) electrochemiluminescence sensor based on silica nanoparticles doped with a self-enhanced Ru(bpy)32+-carbon nitride quantum dot luminophore, *J. Colloid Interface Sci.*, 2022, **608**, 1151–1161.

34 Q. Zhang, Y. Liu, Y. Nie, Y. Liu and Q. Ma, Wavelength-Dependent Surface Plasmon Coupling Electrochemiluminescence Biosensor Based on Sulfur-Doped Carbon Nitride Quantum Dots for K-RAS Gene Detection, *Anal. Chem.*, 2019, **91**, 13780–13786.

35 M. Esmaeilzadeh, S. Sadjadi and Z. Salehi, Pd immobilized on hybrid of magnetic graphene quantum dots and cyclodextrin decorated chitosan: An efficient hydrogenation catalyst, *Int. J. Biol. Macromol.*, 2020, **150**, 441–448.

36 D. Dorokhin, S.-H. Hsu, N. Tomczak, C. Blum, V. Subramaniam, J. Huskens, D. N. Reinhoudt, A. H. Velders and G. J. Vancso, Visualizing Resonance Energy Transfer in Supramolecular Surface Patterns of β-CD-Functionalized Quantum Dot Hosts and Organic Dye Guests by Fluorescence Lifetime Imaging, *Small*, 2010, **6**, 2870–2876.

37 K. Bodenhöfer, A. Hierlemann, M. Juza, V. Schurig and W. Göpel, Chiral Discrimination of Inhalation Anesthetics and Methyl Propionates by Thickness Shear Mode Resonators: New Insights into the Mechanisms of Enantioselectivity by Cyclodextrins, *Anal. Chem.*, 1997, **69**, 4017–4031.

38 B. Chankvetadze, Combined approach using capillary electrophoresis and NMR spectroscopy for an understanding of enantioselective recognition mechanisms by cyclodextrins, *Chem. Soc. Rev.*, 2004, **33**, 337–347.

39 S.-Y. Wang, L. Li, Y. Xiao and Y. Wang, Recent advances in cyclodextrins-based chiral-recognizing platforms, *TrAC, Trends Anal. Chem.*, 2019, **121**, 115691.

40 Y. He, F. Hu, J. Zhao, G. Yang, Y. Zhang, S. Chen and R. Yuan, Bifunctional Moderator-Powered Ratiometric Electrochemiluminescence Enzymatic Biosensors for Detecting Organophosphorus Pesticides Based on Dual-Signal Combined Nanoprobes, *Anal. Chem.*, 2021, **93**, 8783–8790.

41 J. Y. Chan, H. Zhang, Y. Nolvachai, Y. Hu, H. Zhu, M. Forsyth, Q. Gu, D. E. Hoke, X. Zhang, P. J. Marriot and H. Wang, Incorporation of Homochirality into a Zeolitic Imidazolate Framework Membrane for Efficient Chiral Separation, *Angew. Chem., Int. Ed.*, 2018, **57**, 17130–17134.

42 Y.-M. Lei, W.-X. Huang, M. Zhao, Y.-Q. Chai, R. Yuan and Y. Zhuo, Electrochemiluminescence Resonance Energy Transfer System: Mechanism and Application in Ratiometric Aptasensor for Lead Ion, *Anal. Chem.*, 2015, **87**, 7787–7794.

43 X. Yang, Y.-Q. Yu, L.-Z. Peng, Y.-M. Lei, Y.-Q. Chai, R. Yuan and Y. Zhuo, Strong Electrochemiluminescence from MOF Accelerator Enriched Quantum Dots for Enhanced Sensing of Trace cTnI, *Anal. Chem.*, 2018, **90**, 3995–4002.

44 W. Yao, L. Wang, H. Wang and X. Zhang, Cathodic electrochemiluminescence behavior of norfloxacin/peroxydisulfate system in purely aqueous solution, *Electrochim. Acta*, 2008, **54**, 733–737.

45 O. V. Reshetnyak and E. P. Koval'chuk, A possible scheme of electrochemiluminescence generation on platinum cathodes in aqueous solutions of peroxydisulfates, *Electrochim. Acta*, 1998, **43**, 465–469.

46 W. Oi, M. Isobe, A. Hashidzume and A. Harada, Macromolecular Recognition: Discrimination between Human and Bovine Serum Albumins by Cyclodextrins, *Macromol. Rapid Commun.*, 2011, **32**, 501–505.

4248 | *Inorg. Chem. Front.*, 2024, **11**, 4241–4248

This journal is © the Partner Organisations 2024